Journal of South American Earth Sciences 82 (2018) 133–142

Contents lists available at ScienceDirect

Journal of South American Earth Sciences

journal homepage: www.elsevier.com/locate/jsames

Moho depth and equivalent elastic thickness of the lithosphere over the Vema Channel: A new evidence of an aborted ridge

Renata Regina Constantino [a], Iago Sousa Lima Costa [b, *], Peter Christian Hackspacher [a], Iata Anderson de Souza [c]

[a] São Paulo State University – UNESP, Institute of Geosciences and Exact Sciences, Rio Claro, C.P. 178, CEP 13506-900, SP, Brazil
[b] Geological Survey of Brazil – CPRM/DISEGE, Brazil
[c] São Paulo State University – UNESP/UNESPetro, Institute of Geosciences and Exact Sciences, Rio Claro, C.P. 178, CEP 13506-900, SP, Brazil

ARTICLE INFO

Article history:
Received 8 July 2017
Received in revised form
20 December 2017
Accepted 21 December 2017
Available online 26 December 2017

Keywords:
Flexural rigidity
Flexural analysis
Extinct spreading center
South Atlantic evolution
Aborted ridge

ABSTRACT

We investigate the Vema Channel in terms of spatial variations of the elastic thickness (Te) in the frame of the thin plate flexure model using the convolutive method. The modeling of the Moho in terms of the thin plate flexure model is done by a least squares approximation of the Moho obtained from gravity inversion. The flexure is calculated by the convolution of the crustal load with the point-load flexure response curves. The RMS difference between the gravity and flexure Moho surfaces is minimized by varying the Te by inverse modeling. The result is a solution of the flexed crust that is in best agreement with the long-wavelength component of the gravity field.

The flexure Moho depths vary between 12 and 18 km and agree well with those obtained from gravity inversion. The spatial variations of Te range from 2 to 30 km and have a good correlation with the geological interpretation for an aborted ridge near Vema Channel, called in this paper as the Vema Aborted Ridge (VAR). The occurring of seamounts appears to be correlated to a weak and deformed region. Attempts of crustal breakup are marked by high Te values (30 km) while lower values (3–12 km) are found for the suggested aborted ridge. The VAR is on Isochron of 93 Ma and shows symmetrical older along both sides of its axis. Asymmetric magnetic anomalies are found over the ridge and may be related to upper-extended continental crust broken by the Vema.

1. Introduction

The Vema Channel is a large bathymetric feature with more than 750 km of extension and 30 km in width (Mohriak et al., 2010; Fig. 1). The origin of the channel is quite unknown, which makes it an interesting topic for studies aiming to understand the formation and evolution of the South Atlantic Ocean. There are several works addressing paleo-oceanography and water flow (Johnson et al., 1977; Ledbetter and Johnson, 1976), however, geological and geophysical studies are scarce in literature.

According to Bassetto et al. (2000), the development of the whole southeastern Brazilian margin has been conditioned by the action of an N-S-trended oceanic spreading center, and recently, the Vema Channel has been suggested as a potential extinct ridge. Pérez-Díaz and Eagles (2014) proposed an abandoned mid-ocean ridge segment in the South American plate south of the Rio Grande Rise (RGR), which was interpreted at the gravity signal related to the bathymetric trough known as the Vema Channel. They found a strong asymmetry of accreted oceanic crust in the spreading corridor occupied by the trough suggesting that a ridge jump may have occurred. MacLeod et al. (2017) compiled large-scale extinct spreading centers spreads around the world and included the Vema Channel as a possible aborted ridge, although, they suggest that this information should be target for future surveys were additional data must be used to reinforce this hypothesis. Constantino et al. (2017), from a combined analysis of geophysical data, estimated the basement depth for the Rio Grande Rise and interpreted a possible extinct spreading center, which we will call in this paper as the Vema Aborted Ridge (VAR) (Fig. 2) and differs from the morphological structure named Vema Channel.

Bringing new evidences to support the Vema Channel as an

* Corresponding author.
E-mail addresses: renataconstantinobarrella@gmail.com (R.R. Constantino), iago.costa@cprm.gov.br (I.S.L. Costa), phack@rc.unesp.br (P.C. Hackspacher), iataas@rc.unesp.br (I.A. de Souza).

https://doi.org/10.1016/j.jsames.2017.12.011
0895-9811/

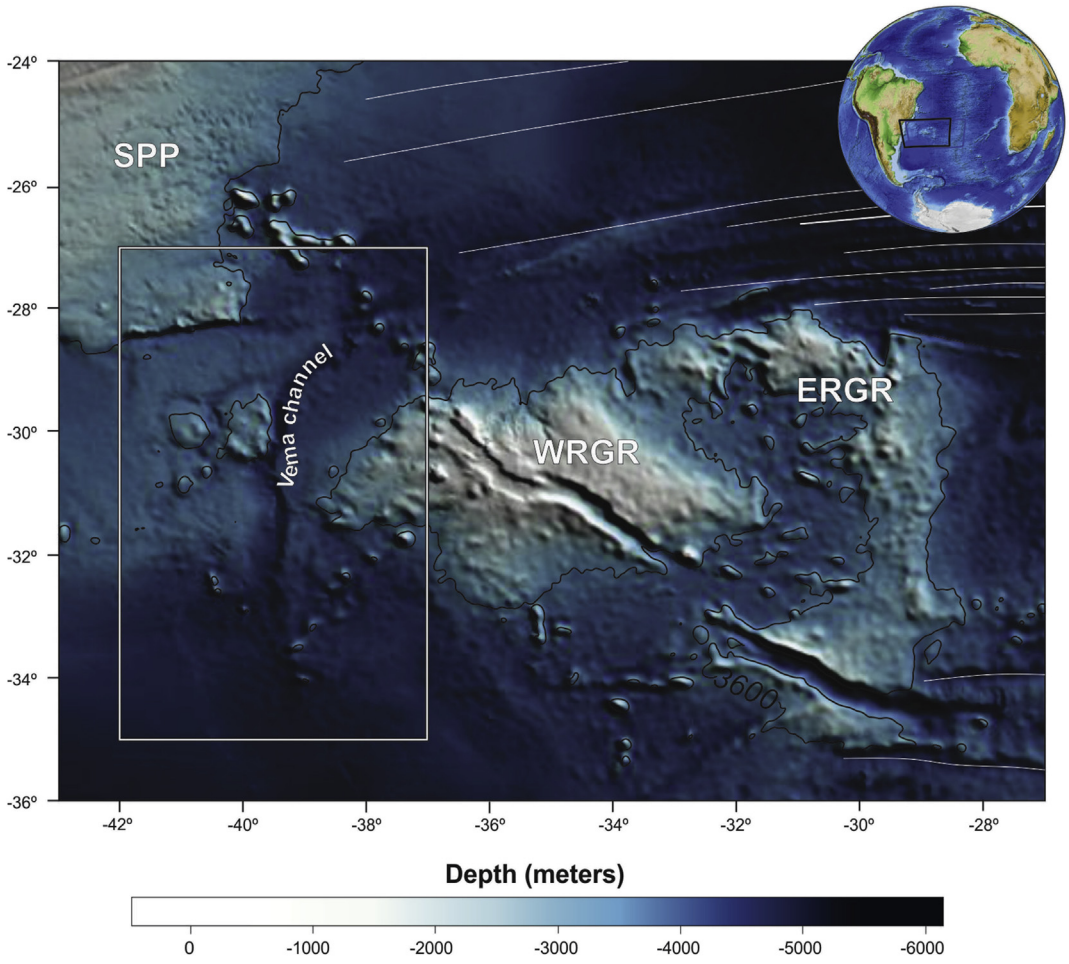

Fig. 1. Bathymetry from ETOPO1 (Amante and Eakins, 2009). The bathymetric isoline of 3600 m is shown. The white rectangle represents the study area. The Vema Channel, the São Paulo Plateau (SPP), the East Rio Grande Rise (ERGR) and West Rio Grande Rise (WRGR) are also represented.

oceanic extinct spreading center (Bassetto et al., 2000; Pérez-Díaz and Eagles, 2014; Constantino et al., 2017; MacLeod et al., 2017), would lead us for a new understanding on the tectonic evolution of the South Atlantic, as well as improving models such as age and spreading taxes of the oceanic crust. A key issue in the understanding of the structure of the extinct ridge is the determination of the spatial variations of the flexural rigidity or equivalent elastic thickness, as it brings implications for how we describe the tectonic processes of a specific area (Pérez-Gussinyé et al., 2004; Kalnins and Watts, 2009). The flexural rigidity is a measure of the resistance of the lithosphere to flexure in response to loading and depends mainly on the elastic thickness (T_e), defined as the thickness of an 'imaginary' elastic plate overlying an inviscid substratum that would bend by the same amount as the 'real' lithosphere under the same applied loads (Tassara et al., 2007).

The lithosphere is assumed to deform elastically in response to suitably old loads according to the thin plate model. The flexural rigidity of the lithosphere is allowed to vary spatially and to have density variations that are considered as internal loads and added to the external bathymetric load (Braitenberg et al., 2003). The modeling of flexure can be accomplished either in the spectral domain or in the spatial domain. Tassara et al. (2007) and Pérez-Gussinyé et al. (2009), using different spectral analyses, produced maps showing the spatial variation of effective elastic thickness for the South America, however previous studies focusing on the particular geological feature of the Channel are not found in the literature. In this paper, the flexure modeling is accomplished in the spatial domain and involves the convolution of the load with the point load response function of the elastic plate model, obtaining the model flexure for the Vema Channel and surroundings. A discussion on the advantages of calculating in the spatial domain can be found in Braitenberg et al. (2002, 2003). The results are compared to the observed flexure of the lithosphere, which is assumed to be equal to the Moho undulations, in this case, obtained by gravity inversion. The solution is a flexed crust that is in best agreement with the long-wavelength component of the gravity field. As by-product of our analysis, we determine the equivalent elastic thickness of the lithosphere.

This work is an extension of Constantino et al. (2017) and therefore, we use part of their results during our procedure: the gravity Moho enters as input data for the flexural analysis and the basement depth is used for discussion of the achieved results. We investigate the Vema Aborted Ridge in terms of rigidity of the crust. Magnetic anomalies and age of the ocean floor are also discussed in order to supplement the hypotheses on the proposed extinct spreading center.

2. Elastic thickness and flexural rigidity

The thin plate flexure model predicts that the outermost layers of the earth respond to long term loads (>1 Myr) analogous to a thin elastic plate overlying an inviscid fluid. The loads are made up

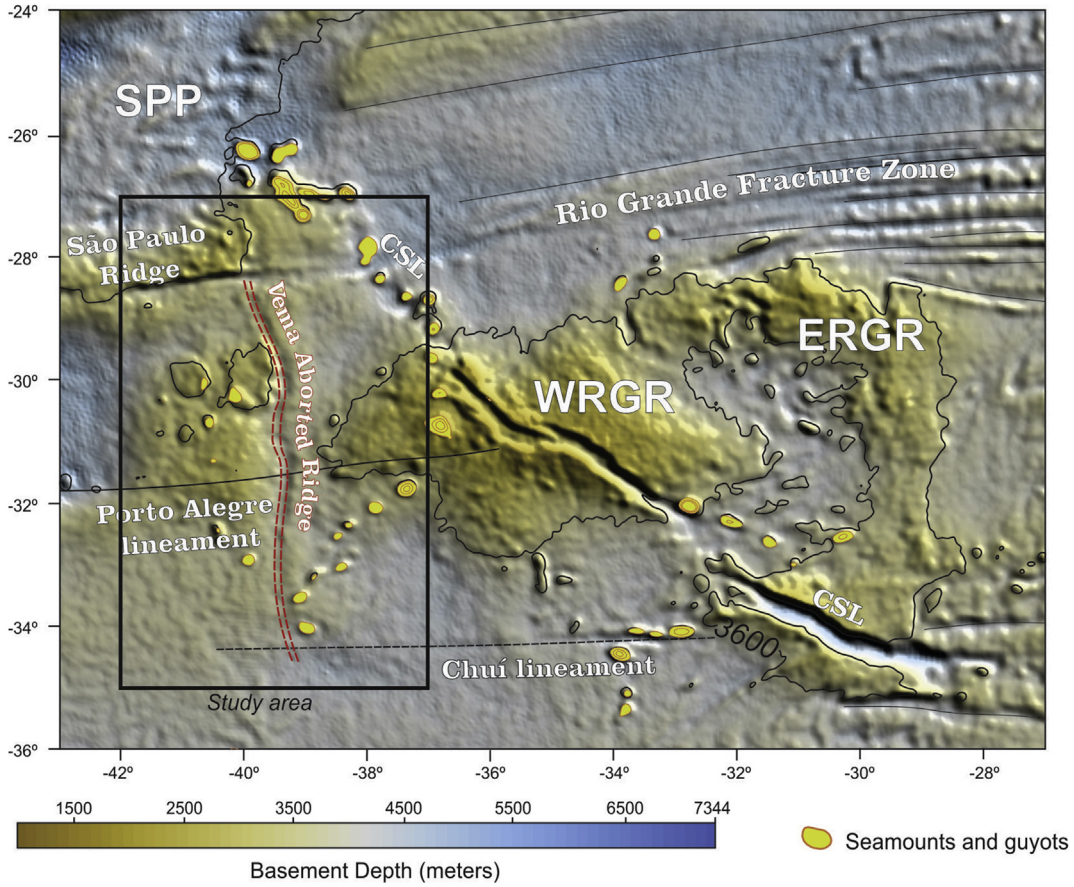

Fig. 2. Basement depth from gravity inversion (Constantino et al., 2017). The black rectangle represents the present study area. SPP – São Paulo Plateau; ERGR - East Rio Grande Rise; WRGR - West Rio Grande Rise; The Rio Grande Fracture Zone, the São Paulo Ridge, the Seamounts and guyots, the Cruzeiro do Sul lineament (CSL), the Porto Alegre lineament and the Chuí lineament are also represented. For reference, the bathymetric isoline of 3600 m is shown. The red dashed lines represent an interpreted extinct spreading axis, called in this paper as the Vema Aborted Ridge (VAR). (For interpretation of the references to colour in this figure legend, the reader is referred to the Web version of this article.)

of the sum of the topographic and subsurface loads (Karner and Watts, 1983; Braitenberg et al., 2006). The flexure $w(\vec{r})$ of a plate loaded by $h(\vec{r})$, in the space domain is, according to Watts (2001) and Turcotte and Schubert (1982):

$$W\left(\vec{k}\right) = \frac{\rho_c}{\rho_m - \rho_c + \frac{D}{g}\left|\vec{k}\right|^4} H\left(\vec{k}\right) \quad (1)$$

Where $\vec{r} = (x,y)$, $W(\vec{k})$ is the Fourier transform (FT) of the flexure $w(\vec{r})$ of the plate, $H(\vec{k})$ is the FT of topography, ρ_c, ρ_m, are respectively the crust and mantle densities, g is the normal gravity acceleration, $\vec{k} = k_x, k_y = 2\pi(v_x, v_y)$ is the two-dimensional wavenumber, v_x, v_y are the spatial frequencies along the x and y axis, respectively and D is the flexural rigidity of the plate: a parameter that characterizes the apparent flexural strength of the lithosphere, defined in terms of Young's modulus (E), Poisson's ratio (υ) and equivalent elastic thickness (Te) with the following equation:

$$D = \frac{ETe^3}{12(1-\nu^2)} \quad (2)$$

In this paper we refer to the elastic thickness instead of to the flexural rigidity, which implies a choice of a rheological model and elastic thickness must be scaled accordingly to this model. The deflection of the plate depends on the properties of the plate, or in other words: how resistant is the material of the plate against a deformation (Wienecke, 2006).

By taking the Fourier inverse transform of Eq. (1), the relation between the two quantities is given in space by the relation:

$$w(\vec{r}) = s(\vec{r}) * h(\vec{r}) \quad (3)$$

where is the convolution product of the load $h(\vec{r})$ with the point load flexure response function $s(\vec{r})$.

In the thin plate flexure model, it can be assumed that the flexure w $(\vec{r})$ approximately equals the deviations from the flatness of the Moho interface. By using a series of flexure functions in the convolution, we obtain the corresponding undulation of the flexure Moho. The response functions are calculated through the 2D inverse Fourier transform (FT) of the flexure defined by equation (1) and the model flexure is compared to the observed flexure of the lithosphere. For this paper, the observed Moho is assumed to be the one obtained from gravity inversion.

To compute the spatial variations of Te, the root mean square (RMS) difference between the observed Moho and the flexure Moho is determined on square windows of side lengths L. The inverted Te for the set window is the one that minimizes the RMS error, and therefore achieves the best-fit approximation of the observed Moho (Braitenberg et al., 2003).

3. Estimation of Moho from gravity inversion

The modeling of the Te is made by a best fit of the flexure Moho with an independent Moho. For this paper, we use the model obtained by Constantino et al. (2017) and remapped for the study area (Fig. 3).

For the estimation of Moho depth, a database of sediment thickness (Divins, 2003), bathymetry (Amante and Eakins, 2009) and free-air anomaly (Sandwell et al., 2014) is used. Since sedimentary packages over the oceans can produce a long wavelength gravity signal, the first point is to remove its effect from the gravity signal. The gravity effect of the sediments is calculated by Parker algorithm (Parker, 1973), which can be done with a constant density contrast along the discontinuity, or, for more realistic results, considering the sediment compaction with depth. For the study, a linear compaction model is considered (Wienecke et al., 2008) and the parameters are controlled by drilling logs from Deep See Drilling Project (Barker, 1983).

The gravity effect of sediments is then subtracted from the Bouguer anomaly, and the resulting gravity field is inverted according to the methodology proposed by Braitenberg et al. (1997). For the inversion process, three initial parameters must be defined. The cutoff wavelength that limits the wave number range used in the inversion is estimated from the decay of the amplitude spectrum of the gravity field (Russo and Speed, 1994). Seismic investigations are used as constraints for the choice of the two other parameters, the reference depth (d) and the density contrast ($\Delta\rho$). The best agreement (minor RMS) between the seismic punctual values and the results obtained from the gravity inversion procedure, determines the couple of d and $\Delta\rho$. The result is a gravity Moho constrained from seismic data.

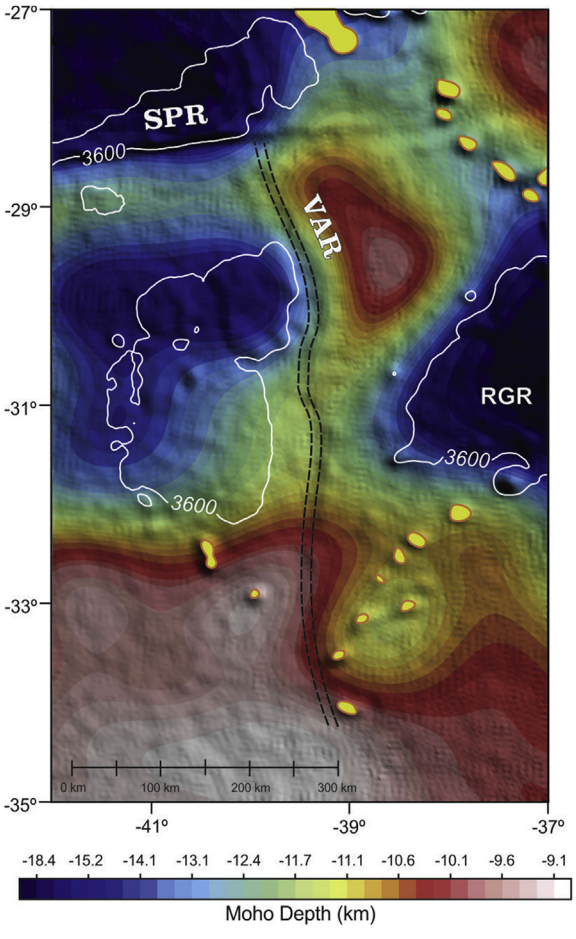

Fig. 3. Moho from Gravity inversion (Constantino et al., 2017), superposed on the basement topography. RGR – Rio Grande Rise; Seamounts and Guyots (yellow with red contours); The São Paulo Ridge (SPR) and the Vema Aborted Ridge (VAR) are also represented. For reference, the bathymetric isoline of 3600 m is show in white contours. (For interpretation of the references to colour in this figure legend, the reader is referred to the Web version of this article.)

4. Flexural modeling

We first apply the methodology introduced in Braitenberg et al. (2003) to calculate the crustal load which consists of the sum of the topographic load and the intracrustal load, the latter considered in this study as the load of the sediments. The total equivalent topography (Fig. 4), defined as the height or depth that the crust will assume in the absence of water and under isostatic conditions (Kumar et al., 2011), is calculated with equation (4).

$$H_{eq} = \left(H_{bathy}\frac{\rho_c - \rho_w}{\rho_c}\right) + \frac{L_{buried}}{\rho_c} \quad (4)$$

Where L_{buried} is inner-crustal loads, H_{bathy} is the bathymetry, ρ_c and ρ_w are respectively the crust and water densities. The load is negative because over oceanic areas, the water-filled is lighter than the reference crust. The same is valid for the sediments, on condition that the density is less than the crustal reference density (Braitenberg et al., 2006).

The flexure is computed by applying the convolution product of the load with a set of flexure response curves, ranging from

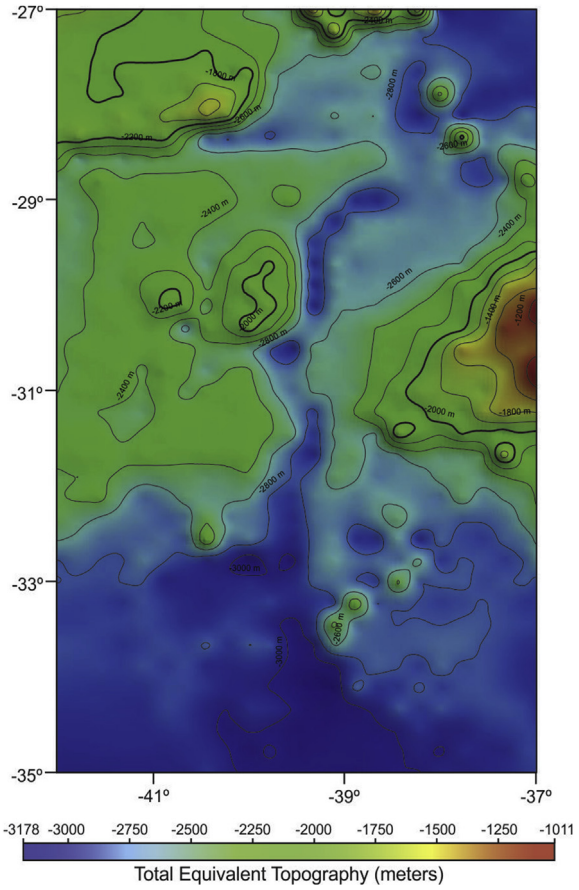

Fig. 4. Total load given by the sum of topographic and intracrustal loads over the study area expressed in terms of equivalent topography.

Te = 0 km to Te = 30 km at a step of 1 km. The convolution radius varies in function of the elastic thickness between 25 and 324 km. This parameter depends on the elastic thickness and density contrast between the plate and the underlying layer. The radius of convolution increases for increasing elastic thickness because of a rise in the rigidity of the plate, therefore, greater elastic thickness values require a greater convolution radius. We refer to Wienecke (2006) on the estimation of this parameter.

The flexed surfaced is compared to the gravity Moho. The Te is fitted in order to obtain the minimum of the RMS difference between the flexure and the gravity Moho. The analysis is carried out on square windows of side length L that are shifted by a quantity ***l***. The L determines the spatial resolution with which the Te is modeled. The lower the value assigned to L, the higher the resolution. Very small values can make unstable results and big values can mask the existing spatial variations of the elastic thickness, so, tests must be made to achieve results that satisfy both conditions. The parameter *l* should be chosen in consideration of the grid node distance of the input grids in order to cover the entire investigated area. From tests made with different values, we found that 100 km shifted by 20 km is adequate for the conditions of the studied area.

We use standard parameters for the Young modulus (E = 100 GPa), the Poisson ratio (0.25), 3300 kg/m^3 and 2800 kg/m^3 for mantle and crustal densities, respectively.

The flexure Moho is displayed in Fig. 5a and the difference between the flexure and the gravity Moho is displayed in Fig. 5b. The elastic thickness variations are displayed in Fig. 6.

5. Discussion

The flexure resembles the gravity Moho very closely, as can be verified by comparison of Figs. 3 and 5a. The difference between the two depths is mostly limited to 2 km, as is shown in Fig. 5b. The misfit in Moho undulations is highest in the southwestern part of the investigated area where the gravity Moho is shallower. The estimation of the gravity Moho was done for a laterally constant density contrast, as showed for Constantino et al. (2017). The density contrast acts as a linear scaling parameter to the undulations of the Moho with respect to the reference depth. If available, different values can be used to constrain the model, but that was not the case. If the real density contrast were greater (or smaller) than the one used in the inversion procedure, the deviation of the Moho from the reference depth would result in its depth being overestimated (or underestimated).

The elastic thickness variation ranges from 2 km to 30 km, as displayed in Fig. 6. The Florianopolis Fracture Zone (FFZ) has values from 2 km to 12 km. A localized lower value is found for the VAR (about 3 km). Higher values of Te (30 km) are found on both sides of the VAR, being greater in the western part of the channel, and to the South, along a flat ocean bottom. A good correlation between lower elastic thickness values and the occurring of seamounts is obtained and might represent a weak and deformed region beneath this load (Wessel, 1993). The Te for the seamounts are well correlated with Watts et al. (2006), where they classified some seamounts over the area as “on-ridge” (0 < Te > 12 km) and also as “Flank ridge” (12 km < Te > 20 km). An exception, with high Te values, is found northeast of the study area, under part of Jean Charcot Seamounts (JCS); however, to provide a better discussion over the JCS, the sampling area should be expanded.

Elastic thickness models for the South America have been published for Pérez-Gussinyé et al. (2009) and Tassara et al. (2007). Although both papers presents Te values in a much larger scale,

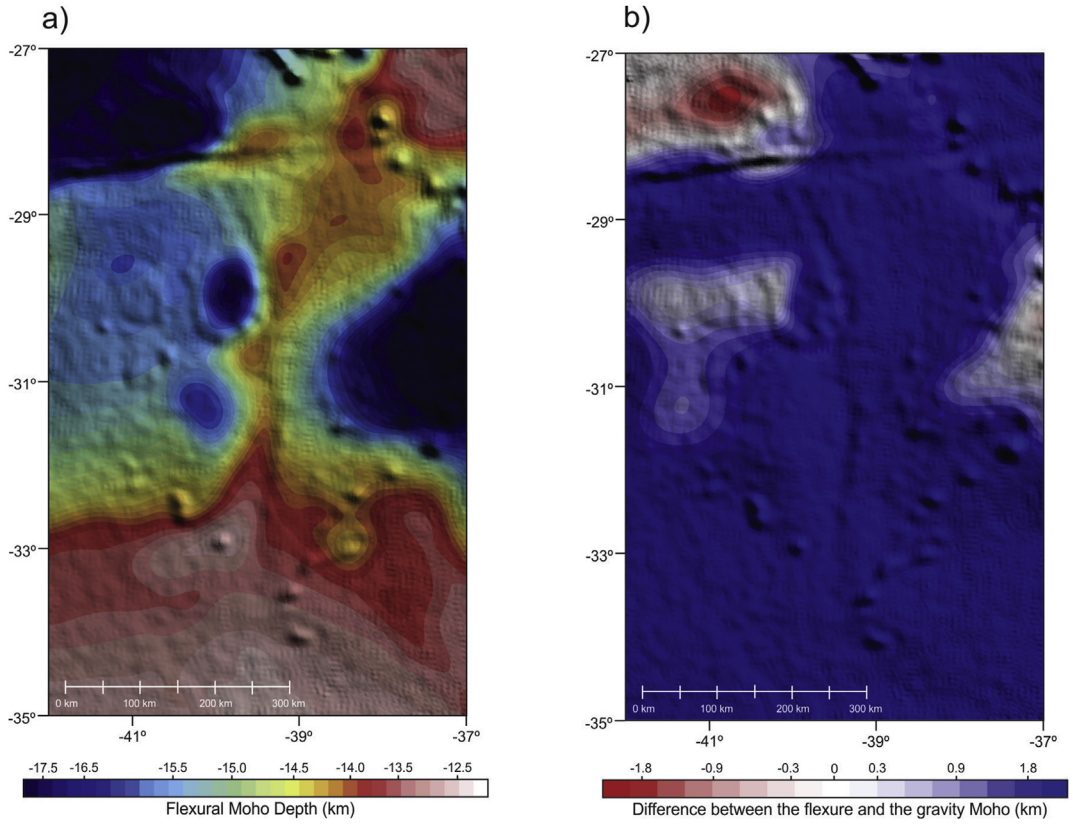

Fig. 5. a) Moho depth obtained from the flexure model; b) Difference between the Moho undulations obtained from gravity inversion and those obtained from the flexure model. For positive values, the flexure Moho is shallower than the gravity Moho. Both maps are superposed on the basement topography.

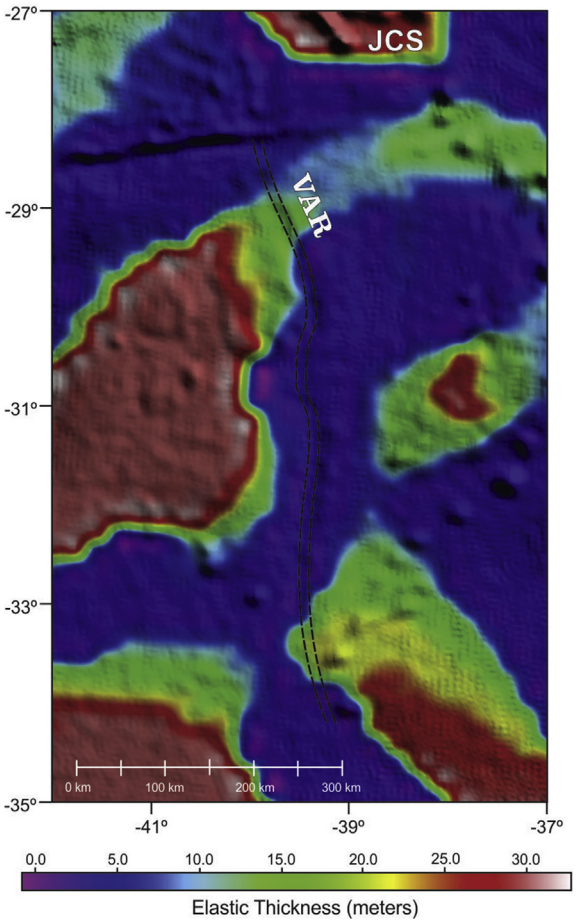

Fig. 6. Elastic thickness superposed on the basement topography. VAR – Vema Aborted Ridge; JCS – Jean Charcot Seamounts.

making difficult to establish a correlation, some available points from Tassara et al. (2007) are compared to our results (Table 1). Small differences of 1 km or less are found for 4 points of comparison, showing great similarity of the models. Higher differences nearly 5 km and 6 km are found for areas with low Te values. While values found in Tassara et al. (2007) are from 7 km to 30 km, lower values are found during this research, starting with 2 km of elastic thickness. Furthermore, as our model evaluate the elastic thickness in intervals of 1 km, it is not possible to estimate uncertainties at smaller intervals. Decimal values are consequence of the grid estimation.

The low values of Te over Vema Channel (Fig. 6) shows that the crustal thickening agrees to that of the thin plate with low rigidity, near to an Airy type local isostatic compensation, which could be an indication of the presence of a plate brake (Braitenberg et al., 2002).

Higher elastic thickness values characterize a rigid structure and lower thickness values indicate a weak lithosphere (Wienecke, 2006; Kearey et al., 2013). A low rigidity, due to low elastic thickness values, represents an important support for a possible aborted rigde through VAR, as suggest by Pérez-Díaz and Eagles (2014), Constantino et al. (2017), and MacLeod et al. (2017).

The basement interpretation (Fig. 7b) considers that two attempts to break-up may have occurred before the formation of the Vema Aborted Ridge. Analyzing the Te values on this two "break-up axis", we find a very rigid crust, which could justify an unsuccessful opening attempt. A hypothesis to a particularly strong crust could be due to the competence of a super extended continental crust, which is more brittle. A good correlation between lower elastic thickness values and the VAR can be clearly seen, mostly over the profile A-A′, which shows an abrupt change from high to low Te values right above the trough (Fig. 7c).

It is possible to observe that the axis of the Vema Aborted Ridge interpreted from the gravity basement agrees with the data published by Pérez-Díaz and Eagles (2017) where the magmatism related to the Vema has ceased and occurred the Ridge Jump in the middle of 93 Ma.

Extinct mid-ocean ridges record past plate boundary reorganization, and identifying their location is crucial to develop a better understanding on the main drivers of plate tectonics and also about oceanic crustal accretion. The flexural rigidity over the Vema Channel indicates a weak crust, supporting the theory that there may have been a ridge in the past, probably extinct after 11 Ma of being active (MacLeod et al., 2017). The presence of seamounts directly to the East of the center may reflect significant volcanic activity around the time of the reorganization. It is also possible that the Tristan Hotspot was active at the time of cessation of spreading within the Vema Channel. However, a reconstruction of the South Atlantic plate boundaries would go beyond the scope of the present paper. Although many other recent works provide the opening history of the South Atlantic (e.g. Eagles, 2007; Aslanian et al., 2009; Torsvik et al., 2009; Moulin et al., 2010; Heine et al., 2013), we could not find any information about a extinct spreading center proposed in this article.

Magnetic reversals for ages of the ocean floor (Fig. 7b) are parallel to the VAR, with younger crust near the extinct spreading center, as expected for a ridge that was active in the past. However, analyzing the magnetic anomaly data (Fig. 8a) obtained from the Earth Magnetic Anomaly Grid with 2-arc-minute resolution (EMAG2), Version 3 (Brian et al., 2016), we cannot find evidence of symmetry on both sides of the channel (Fig. 8b). A low resolution of the magnetic anomaly model would be a possible explanation for the asymmetry, but that is not the case. The EMAG2v3 relies solely on the data available and can represents the complexity of the anomalies in oceanic regions with enough accuracy to estimate magnetic symmetries of the ocean floor. Moreover, this asymmetry is also reported by MacLeod et al. (2017). Evaluating globally extinct ridge, the authors have classified three different types of extinct ridges: The "Well-defined", which one of the characteristics is *symmetric magnetic anomalies*, *identified either side of ridge*; the "Controversial", with *anomalies identified on one flank only or in*

Table 1
Comparison between the elastic thickness data obtained by Tassara et al. (2007) and the results obtained in this article.

Longitude	Latitude	Te (km)	Te (km) Tassara et al. (2007)	Absolute difference (km)
−39.01	−32.05	11.3	10.7	0.6
−40.03	−30.79	10.1	9.2	0.9
−41.67	−34.72	29.9	29.5	0.4
−38.74	−31.37	9.7	8.9	0.8
−38.47	−27.36	24.6	28.3	3.7
−39.61	−30.64	2.6	7.7	5.1
−41.43	−28.49	3	8.9	5.9

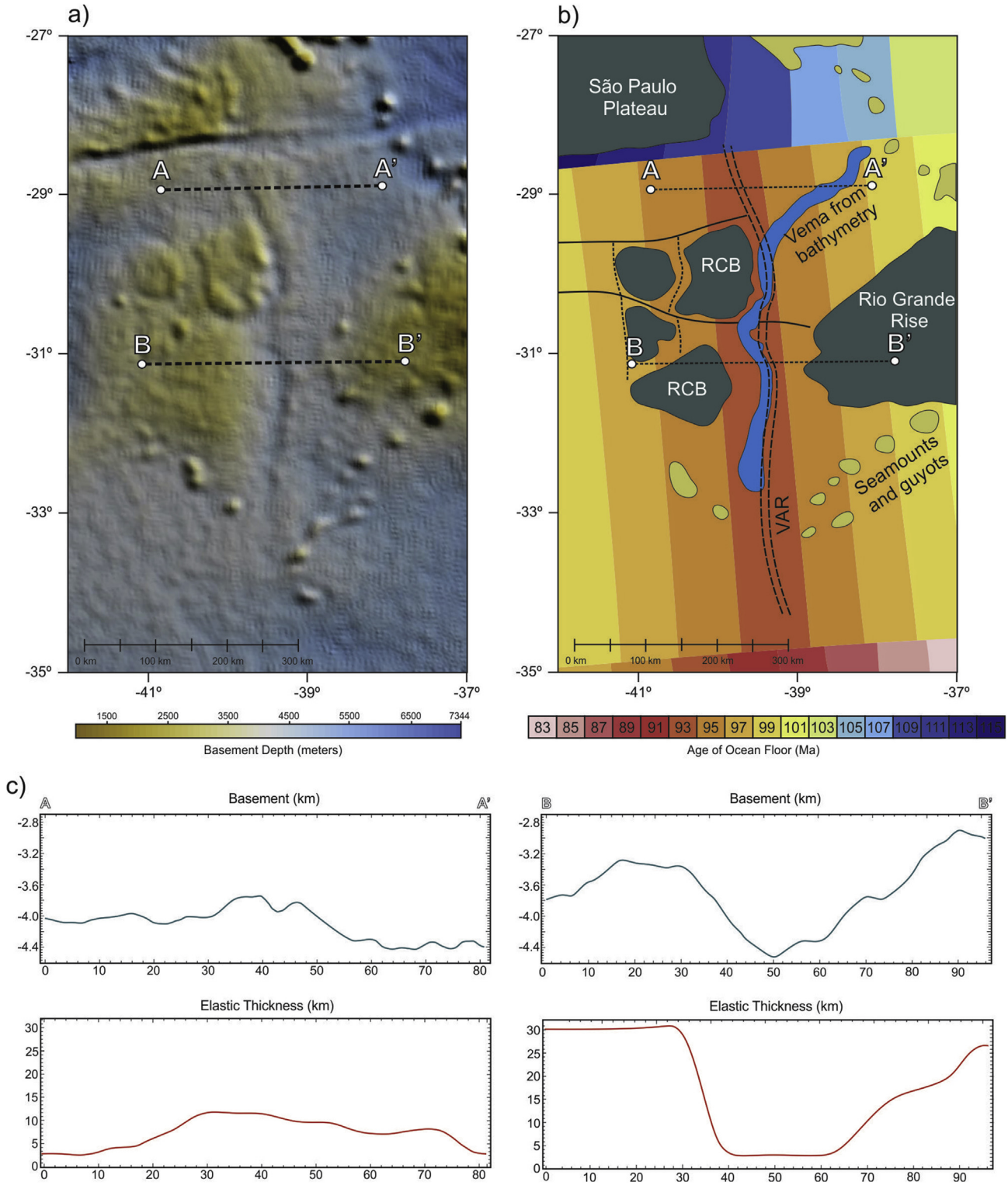

Fig. 7. a) Basement depth from gravity inversion over the Vema Channel (Constantino et al., 2017) and profiles A-A′ and B-B′; b) geological interpretation of the basement over age of the ocean floor from Pérez-Díaz and Eagles (2017). RCB – Rough continental blocks. The dotted lines between the two RCB and parallel to the Vema Aborted Ridge (VAR) may represent two attempts of break-up. The Vema Channel is represented in blue. c) Elastic thickness values (red) and basement depths (blue) for profiles A-A′ and B-B′. (For interpretation of the references to colour in this figure legend, the reader is referred to the Web version of this article.)

surrounding region; and "Poorly-constrained" with no *identified magnetic anomalies in the region of the extinct ridge.* Although they suggest the Vema as a possible aborted ridge, the feature is classified as a "Controversial" that is, without magnetic symmetry, we believe that this asymmetry may be correlated with the composition of a super-extended continental crust broken by VAR (Brune et al., 2014), however, we encourage a specific study for a better discussion.

Müller et al. (2008) showed in a map of crustal accretion a large accumulation to the right of the channel and a symmetrical deficit

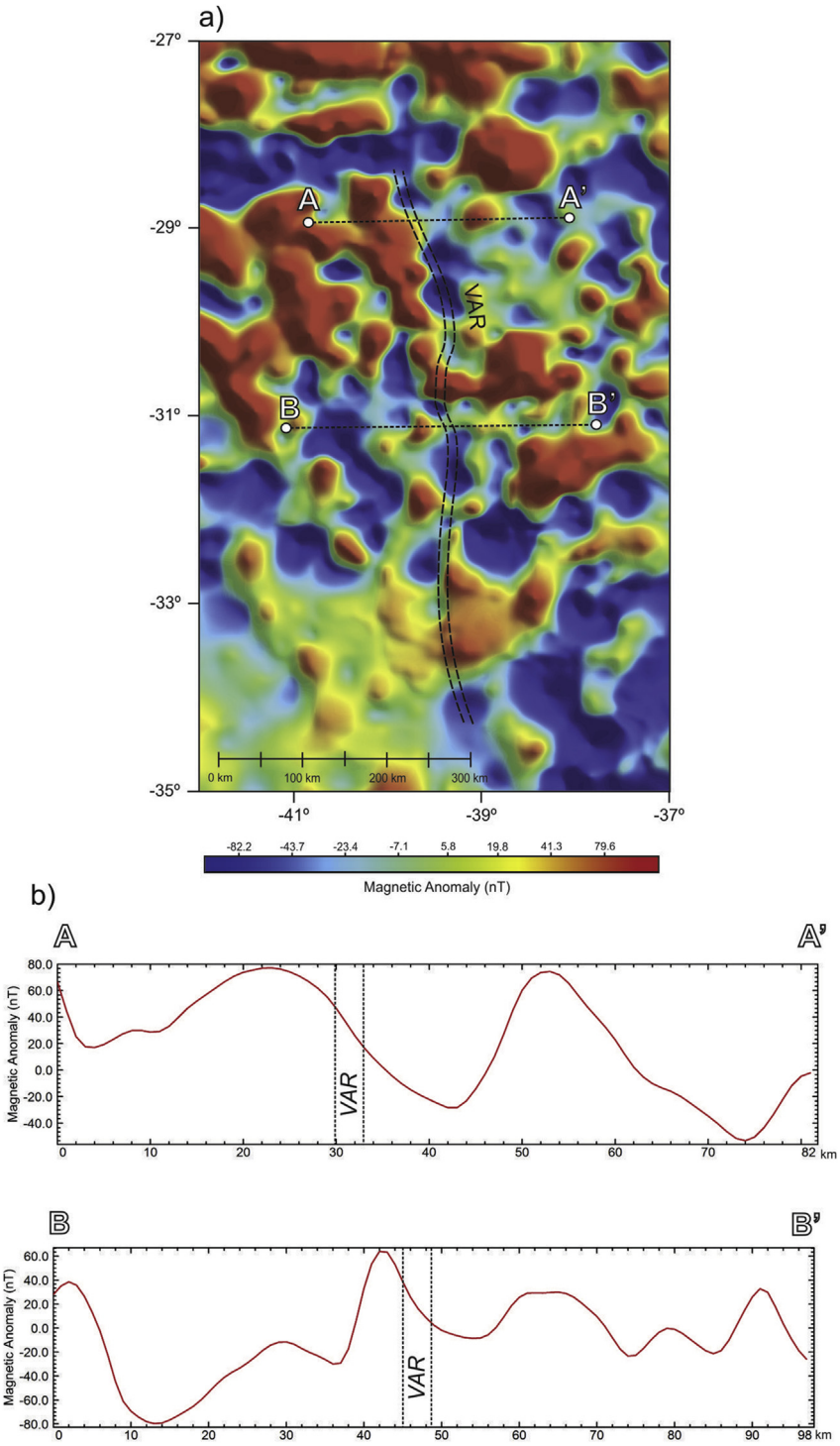

Fig. 8. a) Magnetic anomaly; b) Magnetic anomaly for profiles A-A′ and B-B′.

in the western portion of the African continent. Pérez-Díaz and Eagles (2014) interpreted this asymmetry of accreted oceanic crust as a ridge jump from an aborted rift over the channel.

5.1. Description of the Vema Aborted Ridge (VAR)

After all the points argued in this article, we give a brief description on the proposed aborted ridge. The Vema Aborted Ridge (VAR) is a feature suggested from a basement depth topography model (Constantino et al., 2017) and differs from the Vema Channel, a morphological feature interpreted from bathymetric data (Figs. 1, 2 and 7b). We suggest that the VAR may be related to a western limit of a microplate (pointed partially by MacLeod et al., 2017) limited northward by the Florianopolis Fracture Zone (FFZ) and southward by the Chuí lineament (Fig. 2). This limit could also extend up North if the VAR is similar to that proposed by Constantino et al. (2017); however, we have not yet obtained data to prove that the spreading center extends beyond

the FFZ. The east limit of this suggested microplate may be the same of the east limit of East Rio Grande Rise (ERGR) due to the lack of geomorphological features similar to mid-ocean ridges. So, we could consider this microplate as a portion of crust transferred from the African Plate as a result of a ridge jump, as proposed by Pérez-Díaz and Eagles (2014).

The VAR is above an Isochron of 93 Ma (Pérez-Díaz and Eagles, 2017) with symmetrical older ages on both of its sides (Fig. 7b) and presents asymmetrical magnetic anomalies (Fig. 8). The VAR is also characterized by a high Moho gradient (Figs. 3 and 5a) and by low elastic thickness (Te) (Fig. 6).

6. Conclusion

We draw the following conclusions from this study:

1. The flexure Moho is very similar to the Moho obtained from gravity inversion. The Moho interface responds isostatically to the bathymetry, in the sense that the deep basin is underlain by a thin crust. Very low values of Te over Vema channel shows a thin plate flexural model with low rigidity, near to an Airy type local isostatic compensation, which could be an indication of the presence of a plate brake.
2. The spatial variations of Te correlates well with some of the major features of the study area: the Florianopolis Fracture Zone is characterized by low Te values, while higher values are found in the direction the Rio Grande Rise.
3. Key observations in the study area bring us new evidences of an aborted ridge over the morphological structure known as Vema Channel. Although being geographically very close, the structures are not the same and to differ between then, the name VAR is given to represent the Vema Aborted Ridge.
4. The VAR could be related to a western limit of a microplate that may be limited northward and southward by the Florianopolis Fracture Zone and by the Chuí lineament, respectively. Having in mind the absence of geomorphological features that would define the eastern limit of the microplate, it is suggested that it has the limit defined by the ERGR east limit.
5. From the Moho data, it can be seen that the VAR interpreted by the gravimetric basement defines an important high Moho gradient. The Moho depth varies from 14 km to the West of Vema, until 10 km to the East, being thicker again above the Rio Grande Rise. This bring us the idea that initially the VAR separated a block of crust super extended to the African side, later called RGR, producing oceanic crust to the East. With the cessation of VAR, the RGR was shifted to the Brazil side again, with the current spreading center.
6. From the interpretation of the basement depth (Fig. 7b), we suggest at least two tries to break-up may have occurred before the formation of the Vema Channel. This is supported by the Te results, where high values, representing a rigid crust, are found for the unsuccessful attempts to break and low values are found for the Vema.
7. We have found significant volcanic activity (seamount and guyots) East of the channel and rough continental blocks to the West. This can be evidence that the volcanic activity may shifted after spreading ceased.
8. The VAR interpreted from the basement is above an isochron of 93 Ma reported by Pérez-Díaz and Eagles (2014, 2017) as a nonmagnetic isochron, the Vema Channel Isocrhon (VCI). Symmetric older ages appears on both sides of the Vema Aborted Ridge.
9. Asymmetric magnetic anomalies are found over the ridge and may be related to upper-extended continental crust broken by the Vema.

This article show new evidences that support the occurrence of an aborted ridge (VAR), which could be a trigger for future studies aiming to understand the tectonic evolution of South Atlantic.

Acknowledgments

We acknowledge support from CAPES, in particular CAPES/IODP Proc. 88887.091710 2014-01 for financial support and for the postdoctoral fellowship of Renata Constantino. We are grateful for helpful discussions with Dr. Carlos Eduardo Ganade de Araújo. Profa. Carla Braitenberg for making software available. Prof. Eder Cassola Molina and the Laboratory of Gravimetry and Geomagnetism from University of São Paulo for providing computers for this study. UNESPetro for the permission to use the laboratories. Reviewers and editors for valuable suggestions.

Appendix A. Supplementary data

Supplementary data related to this article can be found at https://doi.org/10.1016/j.jsames.2017.12.011.

References

Amante, C., Eakins, B.W., 2009. ETOPO1 1 Arc-minute Global Relief Model: Procedures, Data Sources and Analysis. US Department of Commerce, National Oceanic and Atmospheric Administration, National Environmental Satellite, Data, and Information Service, National Geophysical Data Center, Marine Geology and Geophysics Division, Colorado, p. 19.

Aslanian, D., Moulin, M., Olivet, J.L., Unternehr, P., Matias, L., Bache, F., Labails, C., 2009. Brazilian and African passive margins of the Central Segment of the South Atlantic Ocean: kinematic constraints. Tectonophysics 468 (1), 98–112.

Barker, P.F., 1983. Tectonic evolution and subsidence history of the rio-grande rise. Initial Rep. Deep Sea Drill. Proj. 72 (DEC), 953–976.

Bassetto, M., Alkmim, F.F., Szatmari, P., Mohriak, W.U., 2000. The oceanic segment of the Southern Brazilian margin: morpho-structural domains and their tectonic significance. Atl. Rifts Continent. Margin. 235–259.

Braitenberg, C., Pettenati, F., Zadro, M., 1997. Spectral and classical methods in the evaluation of Moho undulations from gravity data: the NE Italian Alps and isostasy. J. Geodyn. 23 (1), 5–22.

Braitenberg, C., Ebbing, J., Götze, H.J., 2002. Inverse modelling of elastic thickness by convolution method—the eastern Alps as a case example. Earth Planet Sci. Lett. 202 (2), 387–404.

Braitenberg, C., Wang, Y., Fang, J., Hsu, H.T., 2003. Spatial variations of flexure parameters over the Tibet–Quinghai plateau. Earth Planet Sci. Lett. 205 (3), 211–224.

Braitenberg, C., Wienecke, S., Wang, Y., 2006. Basement structures from satellite-derived gravity field: South China Sea ridge. J. Geophys. Res. Solid Earth 111 (B5).

Brune, S., Heine, C., Perez-Gussinye, M., Sobolev, S.V., 2014. Rift migration explains continental margin asymmetry and crustal hyper-extension. Nat. Commun. 5, 4014. https://doi.org/10.1038/ncomms5014.

Brian, Meyer, Richard, Saltus, Arnaud, Chulliat, 2016. EMAG2: Earth Magnetic Anomaly Grid (2-arc-minute Resolution). Version 3. National Centers for Environmental Information, NOAA. Model. https://doi.org/10.7289/V5H70CVX.

Constantino, R.R., Hackspacher, P.C., de Souza, I.A., Costa, I.S.L., 2017. Basement structures over Rio Grande Rise from gravity inversion. J. S. Am. Earth Sci. 75, 85–91.

Divins, D.L., 2003. Total Sediment Thickness of the World's Oceans and Marginal Seas. NOAA National Geophysical Data Center, Boulder.

Eagles, G., 2007. New angles on South Atlantic opening. Geophys. J. Int. 168 (1), 353–361.

Heine, C., Zoethout, J., Müller, R.D., 2013. Kinematics of the South Atlantic Rift. arXiv preprint arXiv:1301.2096.

Johnson, D.A., Ledbetter, M., Burckle, L.H., 1977. Vema Channel paleo-oceanography: pleistocene dissolution cycles and episodic bottom water flow. Dev. Sedimentol. 23, 1–33.

Karner, G.D., Watts, A.B., 1983. Gravity anomalies and flexure of the lithosphere at mountain ranges. J. Geophys. Res. 88, 10449–10477.

Kalnins, L.M., Watts, A.B., 2009. Spatial variations in effective elastic thickness in the Western Pacific Ocean and their implications for Mesozoic volcanism. Earth Planet Sci. Lett. 286 (1), 89–100.

Kearey, P., Klepeis, K.A., Vine, F.J., 2013. Global Tectonics. John Wiley & Sons.

Kumar, R.T.R., Maji, T.K., Kandpal, S.C., Sengupta, D., Nair, R.R., 2011. Elastic thickness estimates at northeast passive margin of North America and its implications. J. Earth Syst. Sci. 120 (3), 447–458.

Ledbetter, M.T., Johnson, D.A., 1976. Increased transport of Antarctic bottom water in the Vema Channel during the last ice age. Science 194 (4267), 837–839.

MacLeod, S.J., Williams, S.E., Matthews, K.J., Müller, R.D., Qin, X., 2017. A global

review and digital database of large-scale extinct spreading centers. Geosphere 13 (3), 911–949. https://doi.org/10.1130/GES01379.1. GES01379–1.
Mohriak, W.U., Nóbrega, M., Odegard, M.E., Gomes, B.S., Dickson, W.G., 2010. Geological and geophysical interpretation of the Rio Grande Rise, south-eastern Brazilian margin: extensional tectonics and rifting of continental and oceanic crusts. Petrol. Geosci. 16 (3), 231–245.
Moulin, M., Aslanian, D., Unternehr, P., 2010. A new starting point for the South and Equatorial Atlantic Ocean. Earth Sci. Rev. 98 (1), 1–37.
Müller, R.D., Sdrolias, M., Gaina, C., Roes, W.R., 2008. Age, spreading rates, and spreading asymmetry of the world's ocean crust. Geochem. Geophys. Geosyst. 9, Q04006. https://doi.org/10.1029/2007GC001743.
Parker, R.L., 1973. The rapid calculation of potential anomalies. Geophys. J. Int. 31 (4), 447–455.
Pérez-Díaz, L., Eagles, G., 2014. Constraining South Atlantic growth with seafloor spreading data. Tectonics 33 (9), 1848–1873.
Pérez-Díaz, L., Eagles, G., 2017. A new high-resolution seafloor age grid for the South Atlantic. Geochem. Geophys. Geosyst. 18 (1), 457–470.
Pérez-Gussinyé, M., Lowry, A.R., Watts, A.B., Velicogna, I., 2004. On the recovery of effective elastic thickness using spectral methods: examples from synthetic data and from the Fennoscandian Shield. J. Geophys. Res. Solid Earth 109 (B10).
Pérez-Gussinyé, M., Swain, C.J., Kirby, J.F., Lowry, A.R., 2009. Spatial variations of the effective elastic thickness, Te, using multitaper spectral estimation and wavelet methods: examples from synthetic data and application to South America. Geochem. Geophys. Geosyst. 10 (4).
Russo, R.M., Speed, E.R., 1994. Spectral analysis of gravity anomalies and the architecture of tectonic wedging, NE Venezuela and Trinidad. Tectonics 13 (3), 613–622.
Sandwell, D.T., Müller, R.D., Smith, W.H., Garcia, E., Francis, R., 2014. New global marine gravity model from CryoSat-2 and Jason-1 reveals buried tectonic structure. Science 346 (6205), 65–67.
Tassara, A., Swain, C., Hackney, R., Kirby, J., 2007. Elastic thickness structure of South America estimated using wavelets and satellite-derived gravity data. Earth Planet Sci. Lett. 253 (1), 17–36.
Torsvik, T.H., Rousse, S., Labails, C., Smethurst, M.A., 2009. A new scheme for the opening of the South Atlantic Ocean and the dissection of an Aptian salt basin. Geophys. J. Int. 177 (3), 1315–1333.
Turcotte, D.L., Schubert, G., 1982. Geodynamics: Applications of Continuum Physics to Geological Problems, p. 450.
Watts, A.B., 2001. Isostasy and Flexure of the Lithosphere. Cambridge University Press.
Watts, A.B., Sandwell, D.T., Smith, W.H.F., Wessel, P., 2006. Global gravity, bathymetry, and the distribution of submarine volcanism through space and time. J. Geophys. Res. Solid Earth 111 (B8).
Wessel, P., 1993. A reexamination of the flexural deformation beneath the Hawaiian Islands. J. Geophys. Res. Solid Earth 98 (B7), 12177–12190.
Wienecke, S., 2006. A New Analytical Solution for the Calculation of Flexural Rigidity. Doctoral dissertation. Freie Universität Berlin.
Wienecke, S., Mariani, P., Ebbing, J., 2008. LithoFLEX Tutorial. Available in. http://www.lithoflex.org/lithoflex/home/basics/Lithoflex_tutorial.pdf.